Meteoritics & Planetary Science 38, Nr 4, 501–514 (2003)
Abstract available online at http://meteoritics.org

Lunar regolith breccia Dhofar 287B: A record of lunar volcanism

S. I. DEMIDOVA,[1*] M. A. NAZAROV,[1] M. ANAND,[2] and L. A. TAYLOR[2]

[1]Vernadsky Institute of Geochemistry and Analytical Chemistry, Russian Academy of Sciences, Moscow, 119991, Russia
[2]Planetary Geosciences Institute, University of Tennessee, Knoxville, Tennessee 37996–1410, USA
[*]Corresponding author. E-mail: demidova@geokhi.ru

(Received 3 July 2002; revision accepted 9 April 2003)

Abstract–Dhofar 287 (Dho 287), a recently found lunar meteorite, consists in large part (95%) of low-Ti mare basalt (Dho 287A) and a minor, attached portion (~5%) of regolith breccia (Dho 287B). The present study is directed mainly at the breccia portion of this meteorite. This breccia consists of a variety of lithic clasts and mineral fragments set in a fine-grained matrix and minor impact melt. The majority of clasts and minerals appear to have been mainly derived from the low-Ti basalt suite, similar to that of Dho 287A. Very low-Ti (VLT) basalts are a minor lithology of the breccia. These are significantly lower in Mg# and slightly higher in Ti compared to Luna 24 and Apollo 17 VLT basalts. Picritic glasses constitute another minor component of the breccia and are compositionally similar to Apollo 15 green glasses. Dho 287B also contains abundant fragments of Mg-rich pyroxene and anorthite-rich plagioclase grains that are absent in the lithic clasts. Such fragments appear to have been derived from a coarse-grained, Mg#-rich, Na-poor lithology. A KREEP component is apparent in chemistry, but no highlands lithologies were identified.

The Dho 287 basaltic lithologies cannot be explained by near-surface fractionation of a single parental magma. Instead, magma compositions are represented by a picritic glass; a low-Ti, Na-poor glass; and a low-Ti, Na-enriched source (similar to the Dho 287A parental melt). Compositional differences among parent melts could reflect inhomogeneity of the lunar mantle. Alternatively, the low-Ti, Na-poor, and Dho 287A parent melts could be of hybrid compositions, resulting from assimilation of KREEP by picritic magma. Thus, the Dho 287B breccia contains lithologies from multiple magmatic eruptions, which differed in composition, formational conditions, and cooling histories. Based on this study, the Dho 287 is inferred to have been ejected from a region located distal to highlands terrains, possibly from the western limb of the lunar nearside, dominated by mare basalts and KREEP-rich lithologies.

INTRODUCTION

Dho 287 is a recently discovered lunar meteorite (Taylor et al. 2001). The 154 g stone was recovered in the Dhofar region of Oman on January 14, 2001. The main portion (95%) of the stone is a mare basalt (Dhofar 287A); a minor, adjacent portion (~5%) is a regolith breccia (Dhofar 287B). Taylor et al. (2001) and Anand et al. (2003a) have reported petrology, mineralogy, and chemistry of the Dho 287A basalt. Anand et al. (2003a) have demonstrated that Dho 287A is a low-Ti, olivine cumulate, mare basalt, which is highly enriched in late-stage mesostasis. Isotopic studies of Sm-Nd and Rb-Sr (Shih et al. 2002) have indicated that Dho 287A basalt is of hybrid origin and has an age of 3.46 ± 0.03 Ga.

Although Dho 287B is a minor lithology of the meteorite, Taylor et al (2001) have suggested that the Dho 287A basalt may be a single clast of a large regolith breccia, which was destroyed during the ejection from the moon or the meteorite fall. Clast population of the breccia, therefore, could provide additional constraints on the magmatic history of the lunar region sampled by the meteorite and petrogenesis of the Dho 287A and related basaltic rocks. Here, we report on petrology of the Dho 287B clasts and discuss possible genetic relationships among various basaltic lithologies found in the breccia. Preliminary results of this study have been presented by Taylor et al. (2001) and Demidova et al. (2002).

METHODS

A polished thin section (38 mm^2) of Dho 287B was studied using traditional methods of optical microscopy in transmitted and reflected light. Mineralogical investigation of

the clasts were conducted at the University of Tennessee, using a Cameca SX50 Electron Microprobe (EMP) operated at 15 keV and 20 nA with a 1–5 μm beam size and 20 s counting times. Glasses and cryptocrystalline matrices were analyzed with a 10 μm beam size using the same conditions. 10–20 analyses were averaged for each mineral to get a representative composition in each clast. Bulk compositions of the lithic clasts were estimated using average compositions of mineral phases and mineral modes measured by computer reworking of back scattered electron (BSE) images. This technique was applied for the clasts that were large enough to represent a possible bulk-rock composition. Although these reconstructed compositions may have large errors, as discussed below, this technique can yield reasonable approximations of whole-rock compositions.

To establish possible genetic relationships among the Dho 287B basaltic lithologies, equilibrium and fractional crystallization modeling of their bulk compositions were performed using the modified version of the METEOMOD program of Ariskin et al. (1997). This program was specially calibrated relative to the experimental data on crystallization of mare-basalt melts (Green et al. 1971a, 1971b; Grove and Bence 1977; Grove and Vaniman 1978; Walker et al. 1977). Crystallization modeling was carried out at an oxygen fugacity (fO_2) buffer equivalent to iron-wüstite (IW) and 1 atm pressure.

PETROGRAPHY AND MINERAL CHEMISTRY

Dho 287B is a dark lithology forming the top portion of the Dho 287 stone (Fig. 1). The lithology is ~6 mm thick and has a sharp contact with the Dho 287A basalt. Dho 287B is a regolith breccia consisting of a variety of lithic clasts and mineral fragments cemented in a fragmental, fine-grained (<0.1 mm) matrix and minor impact melt. Lithic clasts, of 0.1 to 3.2 mm in size, comprise about 18% of the Dho 287B thin section. These lithic clasts can be subdivided into: 1) crystalline rocks; 2) vitrophyric rocks; and 3) impact-melt breccias. Monomineralic fragments and mineral intergrowths constitute 60–70% of the rock. Rare glass spherules and fragments are also present. The matrix consists of compacted, fine-grained, mineral debris, which are occasionally cemented by impact melt, commonly containing small vesicles.

Representative chemical compositions of mineral phases present in the Dho 287B breccia are listed in Table 1. Mineral chemistries from the Dho 287A basalt (Anand et al. 2003a) are shown in Figs. 3–10 for comparison. Based on genetic relationships, the clasts in Dho 287B are grouped into the following categories: 1) crystalline rocks, which are further sub-divided into low-Ti basalts, VLT basalts, and picritic basalts; 2) vitrophyric rocks; 3) impact-melt breccias; 4) glass spherules; and 5) mineral fragments.

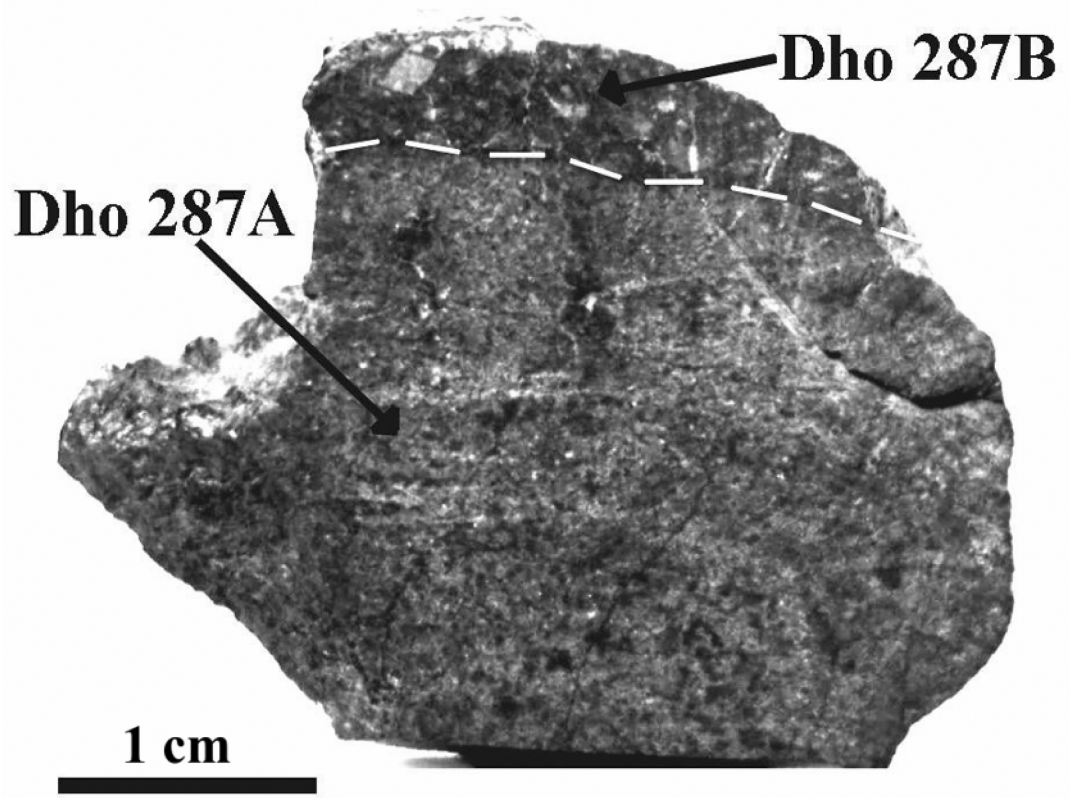

Fig. 1. A cut surface of the Dhofar 287 meteorite. The black lithology on the top of the stone is the Dho 287B regolith breccia.

Table 1. Representative electron microprobe analyses of mineral phases in the Dhofar 287B breccia.

	Low Ti basalts						VLT basalt		
	Clast #7r1		Clast #6r		Clast #5r1		Clast #4r		
	Px	Plag	Px	Plag	Px	Px	Px	Px	Plag
Wt%									
SiO_2	45.8	51.0	48.2	48.7	47.2	41.6	48.3	46.6	45.3
TiO_2	3.62	n.d.[a]	1.56	n.d.	2.23	3.45	0.90	0.71	n.d.
Al_2O_3	4.21	28.4	1.59	30.6	5.22	8.46	4.70	0.57	33.6
Cr_2O_3	0.20	n.d.	0.26	n.d.	1.39	0.02	0.49	0.01	n.d.
FeO	20.4	1.70	24.8	1.16	14.6	29.8	16.9	39.0	1.16
MnO	0.36	n.d.	0.35	n.d.	0.23	0.41	0.31	0.56	n.d.
MgO	7.67	0.61	9.03	0.29	12.2	4.8	11.0	3.79	0.06
CaO	17.1	16.0	13.8	16.5	16.0	10.9	16.5	7.75	18.7
Na_2O	0.05	1.75	0.06	1.62	0.06	0.05	<0.03	0.04	0.63
K_2O	n.d.	0.18	n.d.	0.18	n.d.	n.d.	n.d.	n.d.	0.06
Total	99.4	99.6	99.6	99.1	99.2	99.5	99.2	99.0	99.4
Wo/An	39.2	82.5	30.1	83.9	36.0	26.6	36.7	17.8	94.0
Fs/Ab	36.4	16.3	42.3	14.9	25.6	57.1	29.3	70.0	5.7

	Monomineralic fragments								
	Ol	Ol	Px	Px	Px	Plag	Plag	Chromite	Ulvöspinel
Wt%									
SiO_2	38.7	35.6	53.2	49.5	45.4	52.4	45.0	0.06	0.09
TiO_2	0.05	0.05	0.29	2.08	0.70	n.d.	n.d.	10.2	32.5
Al_2O_3	0.04	<0.03	1.07	3.26	0.61	28.9	33.8	9.14	2.66
Cr_2O_3	0.04	0.23	0.80	0.91	0.01	n.d.	n.d.	39.3	0.26
FeO	20.4	34.3	16.5	11.47	42.6	1.16	1.09	35.6	63.5
MnO	0.24	0.33	0.31	0.26	0.53	n.d.	n.d.	0.18	0.30
MgO	40.6	20.0	24.4	15.1	0.79	0.12	0.12	4.36	<0.03
CaO	0.11	0.34	2.99	17.1	8.6	13.6	19.1	0.22	<0.03
Na_2O	<0.03	<0.03	<0.03	0.11	<0.03	3.10	0.50	n.d.	n.d.
K_2O	–	–	–	–	–	0.22	0.02	n.d.	n.d.
Total	100.2	99.5	99.6	99.8	99.3	99.5	99.6	99.1	99.3
Fo	78.0	59.9	–	–	–	–	–	–	–
Wo/An	–	–	6.0	36.3	19.9	69.9	95.4	–	–
Fs/Ab	–	–	25.9	19.0	77.5	28.7	4.5	–	–

[a]n.d. = not detected.

Crystalline rocks are of basaltic composition, and five fragments of such rocks were found. In terms of chemical composition, two of them resemble low-Ti basalts, another two are very low-Ti basalts (VLT), and one has a picritic composition.

Low-Ti Basalts

Clast #6r is a rounded fragment ~1 mm in its longest dimension (Fig. 2a). This clast consists mainly of pyroxene (63%) and feldspar (30%). Accessory minerals are ilmenite (5%) and silica (2.5%). Pyroxene appears to have been the first phase to crystallize. It occurs as big normally-zoned phenocrysts (up to 0.2 mm) of augite ($Wo_{22–34}En_{28–46}$) or, rarely, pigeonite ($Wo_{10}En_{59}$) embedded into a finer-grained plagioclase-pigeonite groundmass. The pyroxenes are compositionally similar to those of Dho 287A (Fig. 3). The same is true for Ti and Cr contents, but some pyroxenes in this clast are higher in Al and Al/Ti ratios (Figs. 4a–4d). Lath-shaped plagioclases are $An_{81–86}$ in composition, and are slightly enriched in Fe with respect to typical mare basalts (Fig. 7). Ilmenite and silica are associated with feldspar and occur as late-stage phases. In terms of mineral chemistry, this clast is similar to Dho 287A except for the absence of olivine in the former.

Clast #7r1 is a rounded fragment 0.3 × 0.2 mm in size (Fig. 2b). The main minerals present are pyroxene (57%), plagioclase (29%), and ilmenite (7%). Accessory minerals include olivine (3.4%) and silica (3%). Olivine occurs as a single rounded grain (50 μm) and is less magnesian (Fo_{41}) than Mg-rich olivines in the Dho 287A basalt. Pyroxene and lath-shaped feldspar form an ophitic texture, which is fine-grained in places. Pyroxene compositions demonstrate progressive enrichment in FeO from augite to Fe-rich augite ($Wo_{21–39}En_{24–28}$). Augites of $Wo_{35–39}En_{24–28}$ compositions are common in the clast but are atypical for the Dho 287A basalt (Fig. 3). In addition, these pyroxenes are distinctly higher in Ti and Al as compared to those of Dho 287A but have a

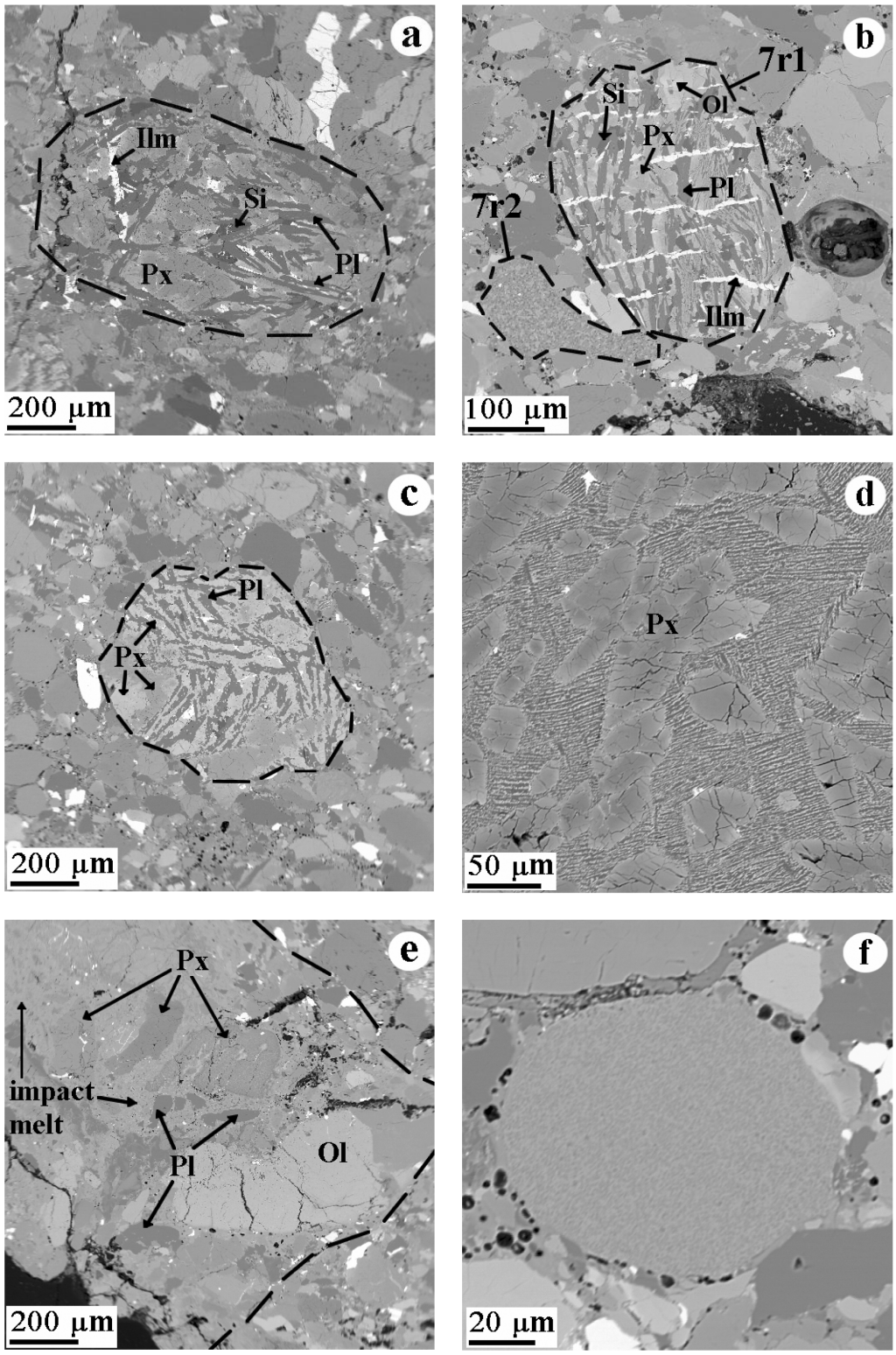

Fig. 2. Backscattered electron images of lithic fragments and glasses from the Dho 287B breccia: a) low-Ti basalt (clast #6r). Pyroxene phenocrysts are set within fine-grained plagioclase-pyroxene groundmass; b) low-Ti basalt (clast #7r1). Subparallel ilmenite crystals cross-cut pyroxene-plagioclase intergrowths. A fine-grained picritic basalt fragment (clast #7r2) is in the lower left corner; c) very low-Ti basalt (clast #4r). Augite phenocrysts occur within ophitic pigeonite-plagioclase groundmass; d) vitrophyric low-Ti basalt (clast # 5r1). Phenocrysts of pyroxene are set within a poorly crystallized matrix; e) impact melt breccia. Single mineral fragments are cemented by poorly-crystallized impact melt; f) glass spherule of picritic composition.

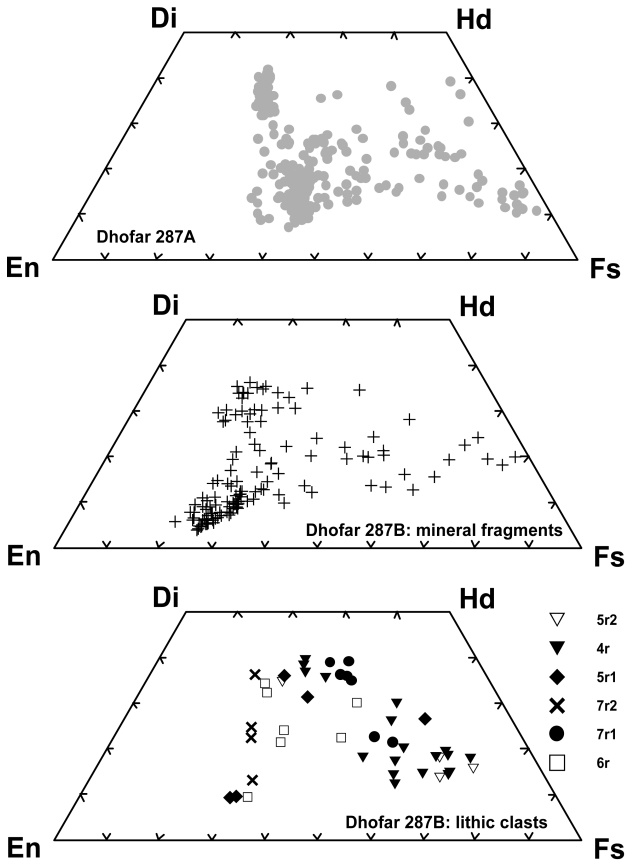

Fig. 3. Pyroxene compositions in Dho 287. Mg-rich pigeonites are present among mineral fragments but were not found in lithic clasts or in Dho 287A.

similar Al/Ti ratio (Figs. 4a–4d). Plagioclase is $An_{81–83}$ in composition with a slight enrichment in Fe (Fig. 7), similar to that in clast #6r described above. Subparallel ilmenite crystals cross the feldspar-pyroxene intergrowths. Silica grains occur mainly within feldspar laths. The textural relationships point to cocrystallization of the major mineral phases. In terms of mineral composition, this clast is similar to Dho 287A, but it does not contain abundant olivine.

Very Low-Ti Basalts

Clasts #4r and 5r2 are similar in texture and mineral compositions and occur as angular lithic fragments of 0.8 × 0.6 mm and 0.3 × 0.2 mm, respectively. These clasts are composed of euhedral augite phenocrysts (up to 0.2 mm) set within an ophitic pigeonite-feldspar groundmass (Fig. 2c). Olivine is absent, and accessory minerals include ilmenite and silica. The mineral modes are: 67–70% pyroxene, 25–30% plagioclase, 1.7% ilmenite, and 1% silica. Augite was the first phase to crystallize, followed by plagioclase and pigeonite. The pyroxene compositions ($Wo_{12–40}En_{12–39}$) are similar to those from clast #7r1 (Fig. 3). In these clasts, pyroxenes are poorer in Ti but have the same or higher Al contents as compared to Dho 287A pyroxenes. As a result, the pyroxenes are characterized by a high Al/Ti ratio, which lowers sharply with a decrease in Mg# [Mg/(Fe + Mg)] (Figs. 4a–4d). Compared to the Dho 287A and Dho 287B low-Ti basalts, these two clasts are distinctly poor in ilmenite and contain plagioclase of high anorthite content ($An_{92–96}$).

Picritic Basalt

Clast #7r2 has an irregular shape and a size of 50 × 200 μm (Fig. 2b). It is a very fine-grained (10–20 μm) rock fragment with an equigranular, granoblastic texture. It is composed of olivine (23%), pyroxene (61%), plagioclase (14%), and chromite (1.6%). The minerals are restricted in composition, in contrast to the crystalline rocks described above. The augites ($Wo_{23–36}En_{44–51}$) and pigeonites ($Wo_{13}En_{56}$) are enriched in Mg (Fig. 3). Olivine is Fo_{59} in composition, similar to many grains in the Dho 287A basalt (Fig. 5). Plagioclase is $An_{91–92}$ and enriched in Fe (Fig. 7). Similar Ca-rich plagioclases are present in the VLT basalt clasts #4r and #5r2.

Vitrophyric Basalts

Three fragments of vitrophyric basalts also occur. These are all similar in texture and mineral compositions. The largest clast, #5r1, is round and equidimensional, about 0.8 × 0.8 mm in size. This is a well-preserved vitrophyric-basalt clast consisting of pyroxene phenocrysts (~50 μm) set in a partially crystallized matrix (Fig. 2d). Pyroxene phenocrysts comprise 49% of the clast; the remainder is groundmass. Pyroxene grains have normal zoning in terms of Mg, Fe, and Ca over a compositional range ($Wo_{27–36}En_{16–38}$), similar to pyroxenes from Dho 287A and other crystalline rocks in the breccia (Fig. 3). However, there is also minor Mg-rich pigeonite ($Wo_{9–10}En_{61–62}$).

Impact-Melt Breccias

There are several fragments of impact-melt breccia in the studied thin section. These are 0.7–3 mm in size and have irregular shapes. The clasts consist of single mineral fragments (up to 0.6 mm) cemented by fine-grained, poorly crystallized impact melt (Fig. 2e). Mineral fragments comprise 10–70% of the clasts and consist of pyroxene, olivine, and plagioclase, with traces of angular grains of ilmenite and chromite.

Glass Spherules and Fragments

Small spherical-glass beads and broken-glass fragments are sparsely distributed, but are characteristic components of the Dho 287B breccia. Glasses, although effectively welding the matrix, are commonly devitrified and vary from 0.1 to

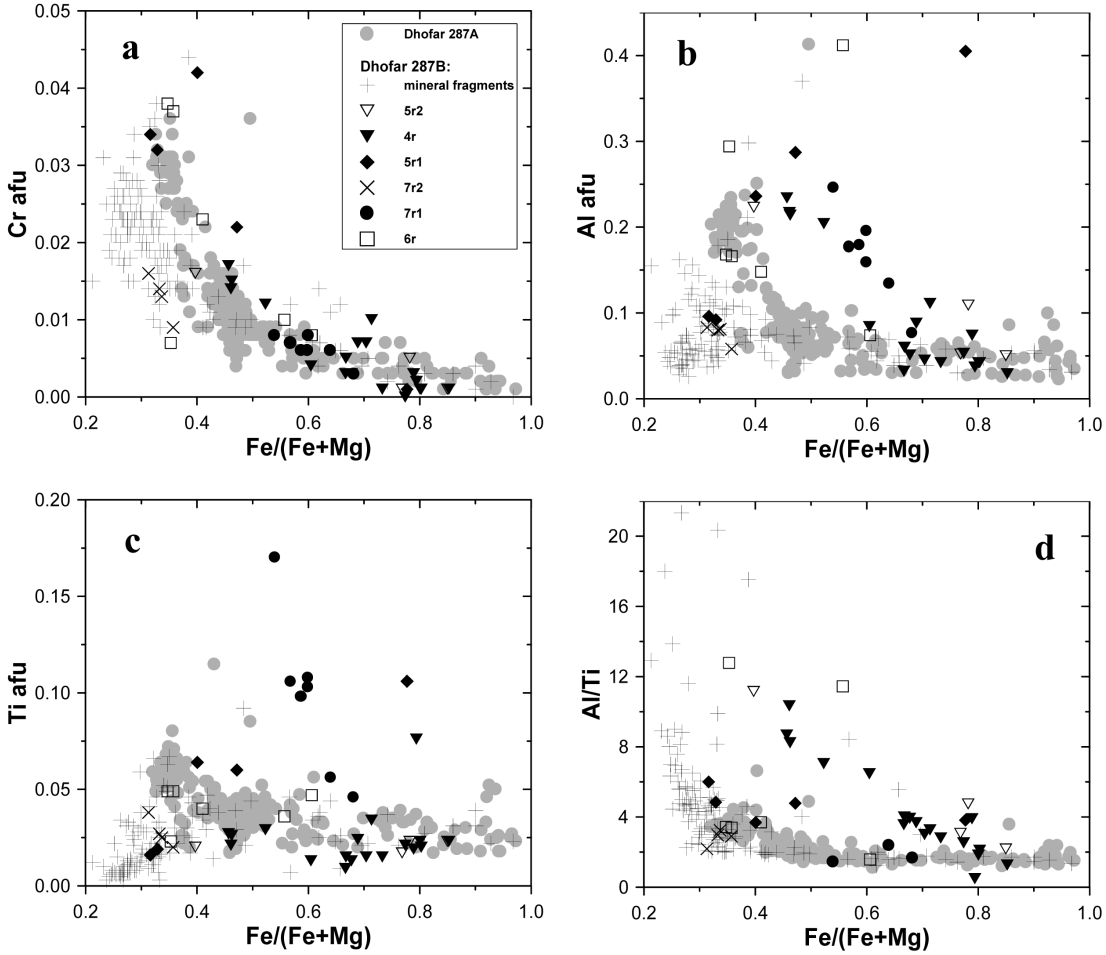

Fig. 4. Cr (a), Al (b), and Ti (c) contents and atomic Al/Ti (d) versus the Fe/(Fe + Mg) atomic ratio in pyroxenes of Dho 287. Atomic formula units (afu) are calculated based on 6 oxygen atoms.

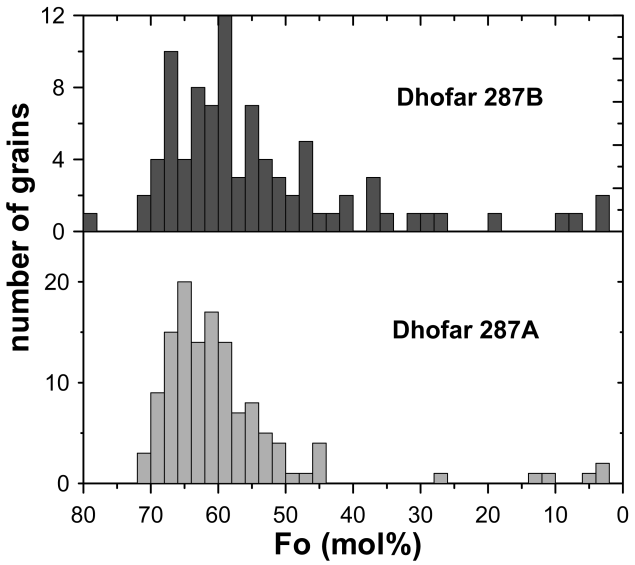

Fig. 5. Histograms of olivine compositions in Dho 287.

0.35 mm in size (Fig. 2f). No schlieren, optically apparent inhomogeneities, or exotic inclusions were found in these glasses.

Mineral Fragments

Discrete angular to rounded mineral grains occur, ranging in size from 0.1 to 1 mm. They are represented mainly by pyroxene, plagioclase, and olivine, with the mafic-mineral fragments more abundant. Minor quantities of chromite, ilmenite, apatite, silica, FeNi metal, and troilite are also present. Rare fragments of a fayalite + K-rich glass mesostasis, described in Dho 287A (Anand et al. 2003a), occur as well.

Generally, pyroxene fragments are similar in composition to those of the Dho 287A mare basalt. However, among Dho 287B mineral fragments, there are abundant high-Mg pigeonites ($Wo_{5–20}En_{60–70}$), which are absent in the Dho 287A and other crystalline rocks (Fig. 3). Only the vitrophyre (clast #5r1) contains minor amounts of pigeonite of similar

composition. The high-Mg pigeonites are unusual for lunar mare basalts. However, such pyroxenes are present in highland rocks, but they are systematically richer in Mg# and usually accompanied by high-Ca, Mg augites, which are not found in Dho 287B. Among lunar mare meteorites, only Y-793274 and EET 96008 contain pyroxenes of similar composition (Arai and Warren 1999; Anand et al. 2003b). These high-Mg pigeonites are also distinct in Cr, Al, and Ti.

In Dho 287B, except among mineral fragments, the Al/Ti ratios in the pyroxenes lower slightly with a decrease in Mg# but tend to a value of 2, typical for lunar pyroxenes (Fig. 4d). In contrast, the high-Mg pigeonites are relatively low in Ti and Al compared with Dho 287A pyroxenes but similar in Cr. In addition, they show a positive correlation between Ti and Mg#. The Al/Ti ratios of the pigeonites are generally high but lower sharply with decreasing Mg#.

Olivine fragments vary from Fo_{78} to Fo_2 in composition. Similar olivine compositions are present in the Dho 287A basalt, but the majority of mineral fragments are slightly richer in intermediate compositions ($Fo_{50–70}$). However, such high-Mg olivines (Fo_{78}) are absent in the Dho 287A basalt (Fig. 5).

Plagioclase has been completely converted to maskelynite, which possesses a huge compositional range from An_{66} to An_{98}, much greater than in the Dho 287A basalt (Fig. 7). In the lithic clasts, the maskelynite compositions show a bimodal distribution in An contents; low-Ti rocks contain plagioclases with lower An contents, while VLT basalts contain relatively An-rich plagioclase grains (Fig. 6). Rare grains, of K, Ba-rich feldspar, occur in mesostasis areas. Some maskelynite fragments in the breccia are relatively enriched in Na, but are not related to mesostasis areas. In terms of Fe content (Fig. 7), maskelynite grains in Dho 287B are not distinguishable from those of Dho 287A and other lunar basalts. Only a few maskelynite grains, which are Ca-rich and Fe-poor, are comparable with lunar highland plagioclases (Fig. 7).

Ilmenite grains analyzed in the Dho 287B breccia and in the Dho 287A basalt are compositionally similar (Fig. 8). In both cases, the ilmenites are both Mg- and Cr-rich (MgO >1 wt%; Cr_2O_3 >0.4 wt%) and Mg- and Cr-poor (MgO <1 wt%; Cr_2O_3 <0.4 wt%). Occasionally, some ilmenite fragments contain inclusions of baddeleyite (ZrO_2). Such inclusions were also identified in ilmenites of Dho 287A.

Among spinel fragments, Cr-rich ulvöspinel is more abundant (Fig. 9) than Ti-rich chromite. Similar ulvöspinel compositions are common in the Dho 287A basalt, which also contains abundant Ti-rich chromites. These Ti-rich chromites in Dho 287B are highly variable in Fe/(Fe + Mg), but display a restricted range in Ti contents (Fig. 9). In contrast, Cr-rich ulvöspinels are characterized by a positive correlation of Fe/(Fe + Mg) and 2Ti/(2Ti + Cr + Al) ratios (Fig. 9). In more Ti-rich ulvöspinel compositions, there are strong depletions in the Cr/(Cr + Al) ratios. The same compositional

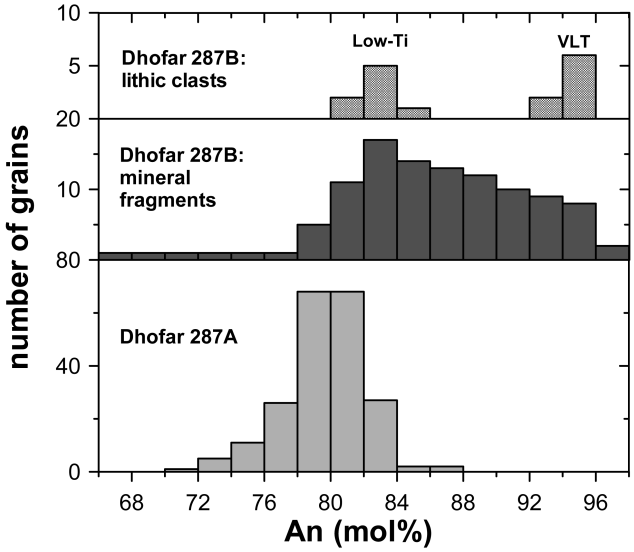

Fig. 6. Histograms of plagioclase compositions in Dho 287.

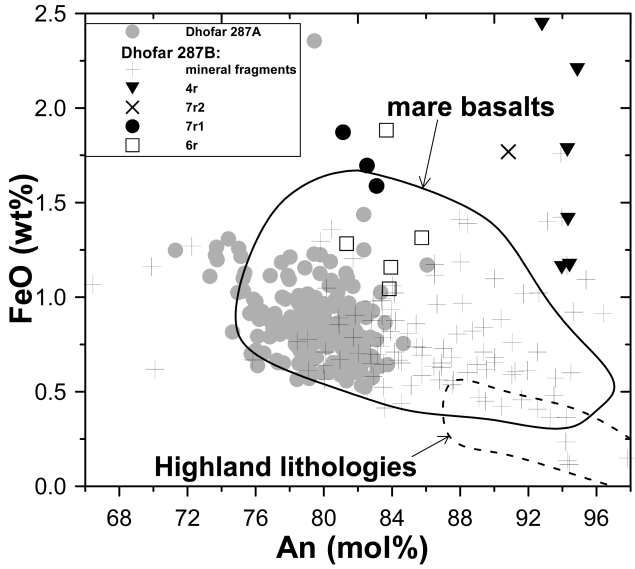

Fig. 7. FeO content in plagioclases of Dho 287. The reference fields are from Stöffler and Knöll (1977) and Papp et al. (1978).

characteristics are typical for spinels of many lunar mare basalts (e.g., Haggerty 1978).

Silica-rich grains contain 0.4–2.6 wt% Al_2O_3, 0.3–0.6 wt% FeO, and up to 0.2 wt% Na_2O and K_2O. This phase is readily identifiable because it exhibits bright-blue luminescence under the electron beam of the EMP, and has the typical crackled texture.

F-rich apatite grains occur as inclusions within fayalite in late-stage mesostasis areas. Such F-apatites are also a characteristic accessory phase of the Dho 287A basalt (Anand et al. 2003a).

On a Ni-Co plot (Fig. 10), FeNi metal grains of the breccia and the Dho 287A basalt are indistinguishable. The

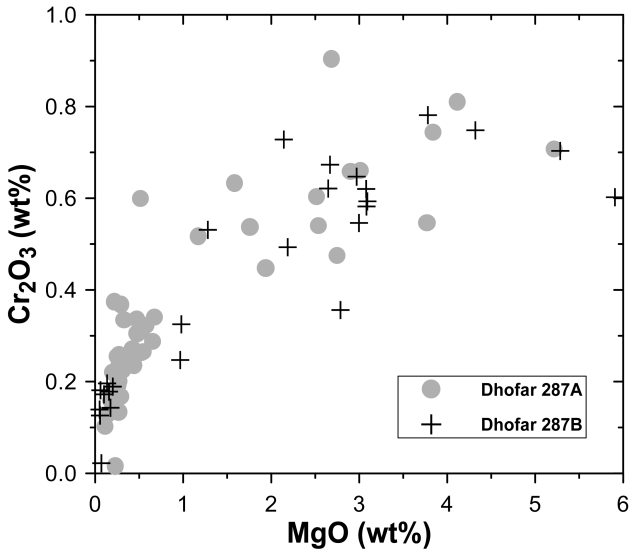

Fig. 8. Mg and Cr content of ilmenites in Dho 287. There are two compositionally distinct clusters in the Dho 287A basalt and the Dho 287B breccia.

grains range in composition from Ni-poor (0.2 wt% Ni) to Ni-rich (54 wt% Ni). Co/Ni ratios of the metal grains are quite variable and most are higher than the cosmic ratio. Most of these FeNi metal grains are of lunar origin, similar to those from Apollo 14, 15, and 16 basalts; the metal grains with Ni contents over 30% are possibly of meteoritic origin, although some polymict rocks (Fig. 10) have similar compositional ranges. Interestingly, P contents of the metal grains are always <0.04 wt%, typical of indigenous lunar FeNi grains from oxygen fugacities just below the IW buffer.

WHOLE-ROCK COMPOSITIONS

Reconstructed whole-rock compositions of crystalline rocks, glasses, and impact-melt matrices are listed in Table 2, along with the data for the Dho 287A mare-basalt from Anand et al. (2003a). In terms of chemical composition (Fig. 11), the basaltic constituents of the Dho 287B breccia can be subdivided into three main groups: 1) low-Ti basalts; 2) very-low-Ti basalts; and 3) picritic basalt.

The low-Ti basalt suite includes clasts #6r and #7r1, the vitrophyre basalt (clast #5r1), and two glass fragments (A and B) (Fig. 11). Impact-melt matrices of the breccia mainly correspond to this group, but their composition could have been significantly modified by mixing processes. The clasts in the low-Ti group are quite similar to Apollo 12 and 15 low-Ti basalts in terms of their Ti content. However, the Dho 287B lithic clasts have relatively higher Na contents, except for the two glasses (A and B), which are similar to Apollo 12 and 15 low-Ti basalts (Fig. 11). The same chemical features characterize the Dho 287A basalt, which is also classified as a low-Ti mare basalt (Taylor et al. 2001; Anand et al. 2003a) enriched in Na, K, and incompatible trace elements. The high-

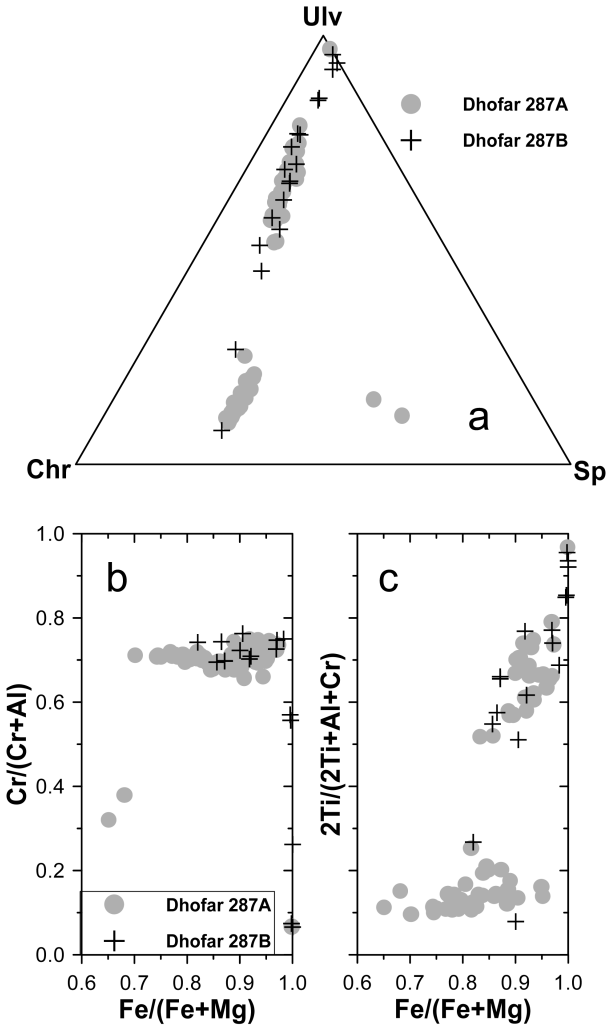

Fig. 9. Major elements composition (a), (b), (c) of spinels in Dho 287.

Na content is normal for high-Ti mare basalts, but is atypical for low-Ti mare basalts (Fig. 11). In addition, enrichment in Na was documented only in Apollo 12 feldspathic basalts, some Luna 16 rocks, and Apollo 14 high-alumina (HA) and very high potassium (VHK) basalts (Neal and Taylor 1992). In the Dho 287B low-Ti basalt suite, the Na-poor glasses (A and B) and Dho 287A are highest in Mg#. These lithologies are also enriched in Cr but depleted in Al and Ca contents (Table 2).

The second group, the VLT basalts, includes clasts #5r2 and #4r and a glass fragment (C). The TiO_2 contents of these clasts (1.4 wt%) are distinctly lower than that of low-Ti basalts but slightly higher than the TiO_2 content of VLT basalts (Fig. 11), which generally contain <1 wt% TiO_2 (Neal and Taylor 1992). However, VLT basalts, containing 1.3–1.44 wt% TiO_2, were described from the Luna 24 VLT basalt suite (Ryder and Marvin 1978; Ma et al. 1978). Therefore, clasts #5r2, #4r, and the glass fragment (C) from Dho 287B can be classified as VLT basalts. The two lithic clasts are low in Mg# as compared to Luna 24 and Apollo 17 VLT rocks and are

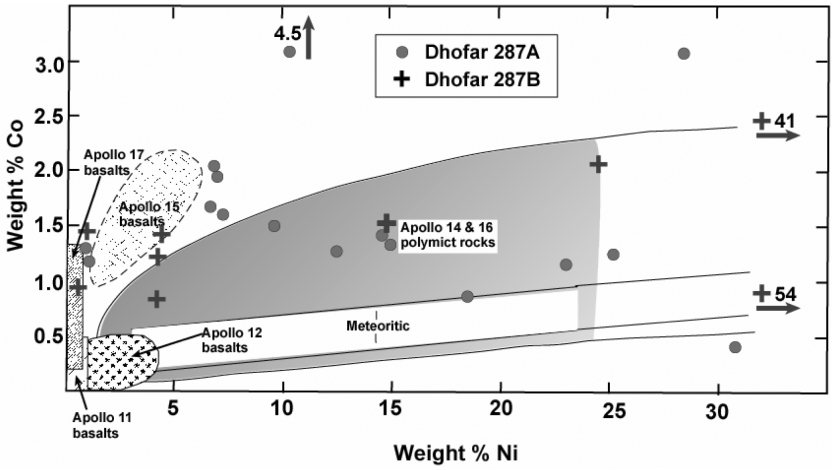

Fig. 10. Ni and Co contents in FeNi metal grains of Dho 287. The reference fields are from Papike et al. (1991).

Table 2. Whole rock compositions of the Dho 287A basalt and Dho 287B lithic clasts and glasses.

	Dho 287A basalt	Low-Ti glasses		Low Ti basalts[a]		Vitro-phyric basalt[a]	VLT basalts[a]		VLT glass	KREEP impact melt breccia[b]	Monzo-diorite glass	Impact melt breccia[b]		Picritic glass
Clast#		A	B	6r	7r1	5r1	5r2	4r	C					
Wt%														
SiO_2	43.9	44.7	46.6	46.6	45.5	47.9	45.8	46.2	47.7	46.3	49.8	44.4	45.7	44.6
TiO_2	2.86	2.80	1.85	3.48	5.39	2.58	1.41	1.44	1.18	1.84	4.12	2.15	3.32	0.64
Al_2O_3	8.10	7.82	7.77	11.5	10.7	10.1	6.14	10.1	12.3	17.5	9.85	12.4	9.49	6.75
Cr_2O_3	0.62	0.50	0.81	0.42	0.14	0.48	0.11	0.17	0.35	0.18	0.25	0.39	0.42	0.53
FeO	22.2	21.5	19.3	15.3	18.28	19.6	29.8	21.6	17.4	10.5	15.6	16.52	20.0	20.9
MnO	0.30	0.28	0.28	0.20	0.28	0.28	0.31	0.29	0.24	0.17	0.23	0.20	0.30	0.29
MgO	12.3	13.2	13.1	8.07	5.65	7.98	5.24	5.95	8.25	9.32	6.21	10.5	8.68	18.3
CaO	8.38	8.53	8.79	11.7	13.0	9.86	9.65	12.7	10.6	11.5	8.84	10.2	10.1	7.31
Na_2O	0.50	0.28	0.32	0.55	0.55	0.47	0.11	0.17	0.45	0.64	0.91	0.48	0.46	0.14
K_2O	0.11	0.05	0.10	0.07	0.07	0.09	0.01	0.02	0.15	0.47	0.96	0.18	0.10	0.04
P_2O_5	n.d.[c]	0.13	0.11	n.d.	n.d.	0.09	n.d.	n.d.	0.20	0.40	1.24	0.21	0.22	0.04
Total	99.5	99.8	99.1	97.9	99.6	99.4	98.5	98.5	98.9	98.8	98.0	97.6	98.8	99.5
Mg#	0.50	0.52	0.55	0.48	0.35	0.42	0.24	0.33	0.45	0.61	0.42	0.53	0.44	0.61

[a]Calculated from mineral modes and averaged mineral compositions.
[b]Matrix compositions.
[c]n.d. = not determined.

also depleted in Na (Fig. 11). However, the VLT glass fragment (C) has relatively higher Mg# and is as high in Na as the rocks of the low-Ti basalt suite.

The picritic basalt group includes the clast #7r2, glass spherules, and glass fragments (Fig. 11; Table 2). The glasses are high in Mg#, low in Ti and Na, and are remarkably similar in composition to Apollo 15 green glasses (Delano and Livi 1981; Steele et al. 1992). They are homogeneous, show a restricted compositional range (Fig. 11), and have Mg/Al ratios (wt%) of 3.0–3.3. Based on the above characteristics, they are classified as volcanic glasses (after Delano 1986), presumably formed by fire-fountain eruptive activity. Clast #7r2 has a similar composition (Table 2), with slightly higher Ti and Ca and lower Al contents relative to picritic glasses. Clast #7r2 is a fine-grained rock that has equilibrated in mineral chemistry and may be a recrystallized picritic glass annealed in pyroclastic or impact deposits.

The presence of abundant Mg-rich pigeonite and high-An grains in the breccia suggests derivation from coarse-grained rock(s). Such rocks may either have formed near the center of an unusually thick lava flow, as in the case of EET 96008 pyroxenes (Anand et al. 2003b), or under hypabyssal cooling conditions. Mg-rich pigeonites, however, are absent in all crystalline lithic clasts of the breccia. Anorthite fragments appear to differ in Fe content from lunar highland-feldspars. Therefore, they could be derived from the Dho 287B VLT lithology that also contains anorthite. This is consistent with the recent studies of lunar meteorites EET 87521 and EET 96008, dominated by VLT basaltic components (Arai et al 1996; Anand et al. 2003b). These meteorites are comprised of

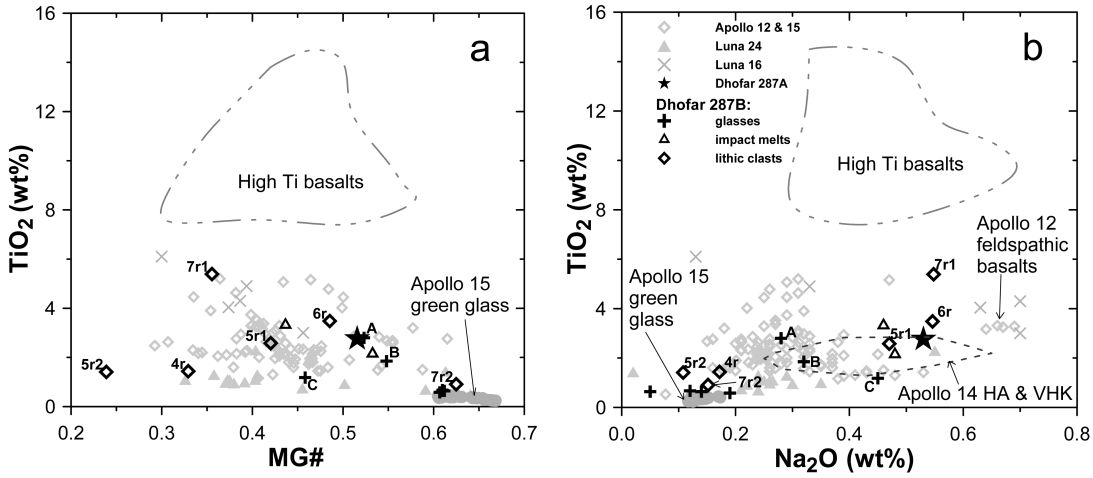

Fig. 11. Mg# versus TiO_2 (a) and Na_2O versus TiO_2 (b) plots for Dho 287B lithic clasts and glasses. Lunar mare basalt compositions are also plotted for comparison (Neal and Taylor 1992 and references therein).

coarse-grained pyroxenes and plagioclase grains, atypical of a mare lava flow, and they also contain Mg-rich pigeonites and anorthite, similar to VLT basaltic clasts of Dho 287B.

In addition to the classified components in Dho 287B, two unusual objects were found. The first one is a glass fragment that is strongly enriched in Si, Na, K, and P (Table 2). The relatively high Mg# (42%) of this fragment distinguishes it from typical late-stage mesostasis of lunar basalts. The glass is compositionally close to Apollo 14 and 15 quartz monzodiorites (e.g., Joliff 1991; Marvin et al. 1991), but as compared to the lithic clasts in the breccia, this glass is higher in Ti. The second object is the matrix of an impact-melt breccia clast. The clast consists of small feldspar fragments embedded in a poorly-crystallized, impact-melt matrix. The matrix has a composition of typical KREEP norites (e.g. Irving 1977). In contrast to the KREEP-rich, late-stage mesostasis of the Dho 287A basalt, this matrix is high in Mg# (61%) and Al_2O_3 (17.5 wt%) (Table 2). KREEP is a characteristic chemical signature in the rocks derived from the western limb of the lunar nearside (e.g., Wieczorek and Phillips 2000). Therefore, the presence of KREEP in Dho 287B helps in identifying a possible source region for this meteorite. Except for this possible KREEP lithology, no other highland-derived components were recognized in Dho 287B. This strongly distinguishes the Dho 287 meteorite from Dhofar 025, found only 400 m away and composed entirely of highland lithologies (Cahill et al. Forthcoming). If these meteorites were paired, the Dho 287B breccia should contain some typical highland material, and the Dho 025 regolith breccia should be contaminated by some mare basalt components of Dho 287. Neither situation occurs.

GENETIC RELATIONSHIPS

Results of the crystallization modeling on several reconstructed whole-rock compositions of Dho 287B clasts and on the measured bulk-composition of Dho 287A basalt (Anand et al. 2003a) show that there may be lithologies representative of two groups of basaltic melts in this breccia. The first group is highly-saturated with olivine and includes picritic lithologies, Dho 287A, and the Na-poor, low-Ti glasses. The second group possibly represents a multi-saturated basaltic melt or very close to cosaturation with olivine, plagioclase, and pyroxene (Figs. 12 and 13). VLT and other low-Ti, Na-rich basaltic lithologies of Dho 287B belong to this group. On the Ol-An-SiO_2 ternary liquidus diagram (Fig. 12), these lithologies plot parallel to the pyroxene-olivine boundary, and most of them are close to plagioclase saturation. It is, therefore, suggested that these rocks could have originated from the more primitive melts of the first group by near-surface olivine fractionation. Such processes are thought to be responsible for a compositional diversity of many mare basalt suites (e.g., Papike and Vaniman 1978; Grove and Vaniman 1978). Anand et al. (2003a) reported that the Dho 287A basalt lithology, although of high Mg# similar to the picritic glass, actually represents that of an olivine cumulate.

Computed equilibrium crystallization of a picritic melt of the Dho 287B breccia (Fig. 13) demonstrates that olivine (Fo_{82}) is the first phase to crystallize followed by olivine (Fo_{69}) + pigeonite (Wo_9En_{67}) and olivine (Fo_{67}) + pigeonite (Wo_9En_{66}) + feldspar (An_{91}). Augite ($Wo_{44}En_{41}$) joins the sequence when 70% of the melt has crystallized. The sequence and the phase compositions are similar to those experimentally obtained for Apollo 15 green glass melts (Grove and Vaniman 1978). Fractional crystallization produces pigeonite (Wo_9En_{61}) and plagioclase (An_{89}) when olivine (Fo_{62}) disappears from the sequence. These results suggest that the population of Mg-rich pigeonite ($Wo_{5–20}En_{60–70}$) and anorthite fragments of the Dho 287B breccia could have formed from a picritic magma. In this scenario, Mg-rich olivine, which would also crystallize from the magma, would have to separate in an

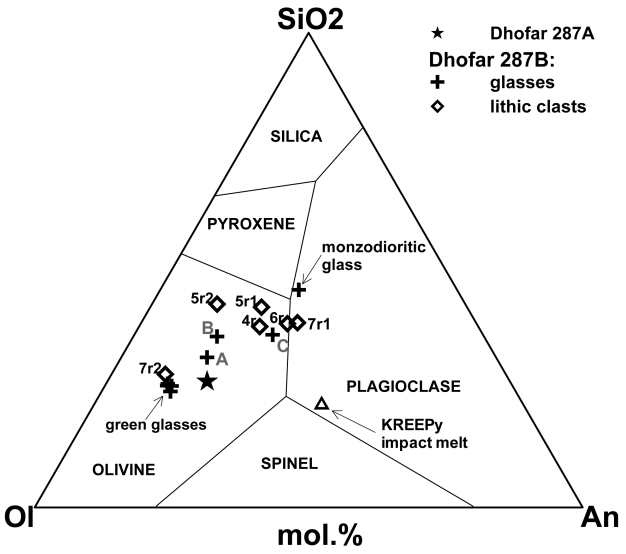

Fig. 12. Compositions of Dho 287 lithologies plotted on the olivine-anorthite-silica pseudo-ternary diagram. Phase boundaries correspond to a Fe/(Fe + Mg) ratio of 0.3 to 0.4 (Walker et al. 1972) at 1 atm pressure. An increase in pressure displaces the olivine-pyroxene boundary toward the Ol apex.

intermediate chamber before eruption of the melt on the surface, an atypical situation. In fact, only one Mg-rich olivine fragment (Fo_{78}) was found in the breccia. Fractional crystallization of the picritic magma can also produce the VLT crystalline rocks of Dho 287B (Fig. 14) but not the Na-rich VLT glass (C) and the low-Ti rocks, which are too enriched in Ti and Na. These enrichments cannot be achieved during fractionation of picritic magma at reasonable degrees of crystallization.

Calculated sequences of equilibrium crystallization of other olivine-saturated melts, i.e., Dho 287A and glasses A and B, are generally similar (Fig. 13): olivine ($Fo_{75–78}$) → olivine ($Fo_{60–68}$) + pigeonite ($Wo_{8–10}En_{60–67}$) + plagioclase ($An_{83–88}$). Augite ($Wo_{45}En_{37}$) appears when 53–67% of the melts have crystallized. Although the Dho 287A could be an olivine cumulate (Anand et al. 2003a), the glasses are texturally similar to the picritic ones and may represent primary melts. Also, the olivine-saturated melts are similar in crystallization sequence, the differences in Na and Ti contents (Fig. 14) indicate that the lithologies could not have originated from the same parent magma, and most of these probably represent independent magmatic episodes. The low-Ti basalt (clast #7r1) can probably be related with the A and B low-Ti glasses by equilibrium crystallization (Fig. 14). However, another low-Ti basalt (clast #6r) is too high in Mg# and Na_2O to have been derived from these melts. Computed, early-formed mineral compositions are higher in Mg# compared to those actually observed in the rock. This suggests that the rock may be a cumulate that originated from another low-Ti parent melt. The vitrophyre (clast #5r1) can be related by magmatic fractionation with the A and B glasses (Fig. 14). The model calculation predicts that the melt is co-saturated with pigeonite and feldspar (Fig. 13), while the rock contains augite and pigeonite phenocrysts set within glassy matrix. This discrepancy may be due to the high-cooling rate of the vitrophyric melt. Fast cooling has been demostrated to suppress feldspar nucleation, leading to augite appearance (e.g., Grove and Bence 1977).

From the above discussion, the whole variety of the basalt lithologies in Dho 287 cannot, apparently, be formed by the near-surface fractionation of a single parental magma. Based on TiO_2 contents (Fig. 14), 3 parent magmas appear to be required, i.e., 1) a picritic melt; 2) a low-Ti, Na-poor melt of glass B composition; and 3) a low-Ti, Na-rich melt similar to that of the Dho 287A bulk-composition. These melts could be generated by variable degrees of partial melting of the lunar mantle. Apollo 15 picritic glasses are believed to have formed by partial melting at depths in excess of 400 km (Grove and Lindsley 1978). The Dho 287B picritic glasses lie on almost the same pyroxene-olivine, high-pressure cotectic that is known to be displaced downward (towards the Ol apex) (e.g., Warren and Wasson 1979) from the low-pressure boundary (Fig. 12), therefore, constraining their source regions to similar depths. The low-Ti, Na-poor glasses have a lower-olivine content (Fig. 12) and, hence, should come from a shallower depth. However, note that significant uncertainties are associated with such estimated depths.

The geochemical differences among the parent magmas may be related to those of the source regions. This can be related to the lateral heterogeneity in the lunar mantle according to the cumulate heterogeneous mantle model proposed by Tanton et al. (2002). Alternatively, the chemical differences among the possible Dho 287 parent magmas could be due to assimilation of KREEP by a picritic magma(s) while rising towards the surface. The model is similar to the dynamic assimilation model of Ringwood and Kesson (1976) and has the following advantages: 1) both picritic and KREEP material occur in the same breccia suggesting that the different types of magmatism occurred in a local region, and, therefore, the spatial association could result in the formation of hybrid melts; 2) the large scatter in Na contents in both VLT (the Na-rich VLT C glass) and low-Ti basalt suites is most compatible with the assimilation model; 3) Dho 287A trace-element characteristics favor contamination by KREEP (Anand et al. 2003a); and 4) Sm-Nd and Rb-Sr isotopic studies (Shih et al. 2002) point to a hybrid composition for the Dho 287A basalt.

SUMMARY

Dho 287B is a regolith breccia dominated by different mare-basalt lithologies. The main lithology is a low-Ti basalt suite that includes Na-rich and Na-poor members. Members of this suite include crystalline rocks, vitrophyres, and glass fragments, each indicative of different cooling histories of lava eruptions. The Dho 287A basalt is also a low-Ti basalt,

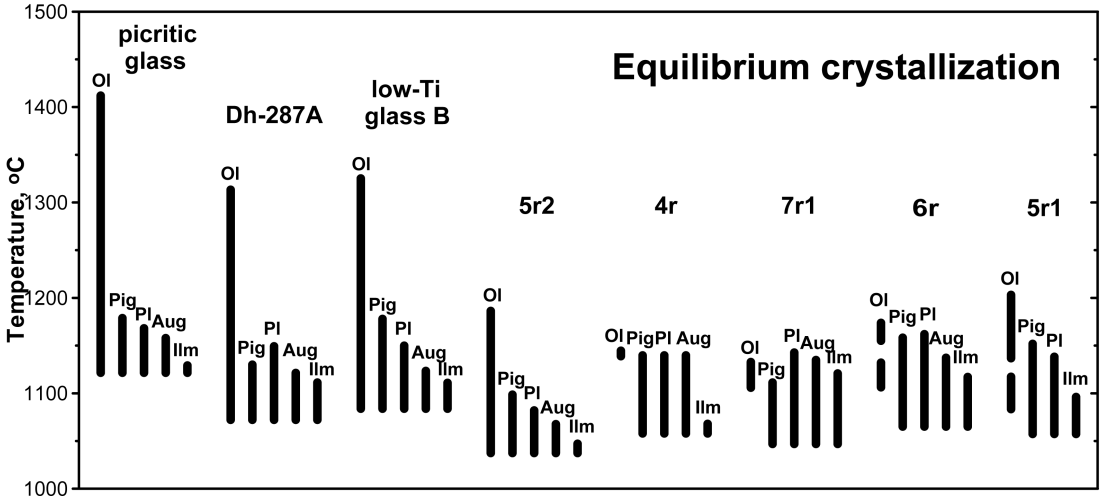

Fig. 13. Results of equilibrium crystallization modeling of Dho 287 rocks and glasses, using the modified METEOMOD program of Ariskin et al. (1997), taken to 95% crystallization. Please, note that the actual measured bulk-composition of Dho 287A is used in this modeling not the olivine-cumulate-corrected, bulk composition of Dho 287A reported by Anand et al. (2003a).

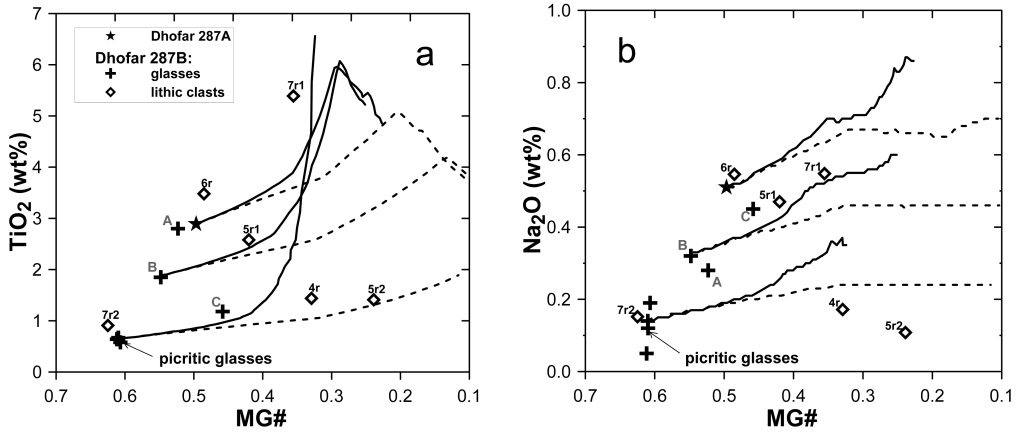

Fig. 14. Plots of Mg# versus TiO_2 (a) and Mg# versus Na_2O (b) showing crystallization paths followed by modeled liquid composition for a Dho 287A-type melt, a low-Ti glass-type melt, and a picritic glass-type melt during equilibrium (solid lines) and fractional crystallization (dashed lines). Please, note that the actual measured bulk-composition of Dho 287A is plotted on this diagram.

and many of the mineral fragments in the breccia were derived from similar lithologies. VLT basalts are also present in the breccia. These clasts are considerably lower in Mg# and slightly higher in Ti, compared to Luna 24 and Apollo 17 VLT basalts. Another minor component of the breccia is the picritic glasses, which are morphologically and compositionally similar to Apollo 15 green glasses, and point to magma eruption with fire-fountain style eruptions in the region sampled by Dho 287. Abundant Mg-rich pyroxene and anorthite mineral fragments are present and are distinct from those present in the lithic clasts. Such mineral fragments were derived from coarse-grained Mg#-rich, Na-poor rocks. Rare KREEP-rich fragments are present, but no typical highland materials were found in the breccia.

The variety of Dho 287 rocks cannot be explained by near-surface fractionation of single parent magma. The picritic glasses, a low-Ti, Na-poor glass, and a low-Ti, Na-rich basaltic melt (similar to that of Dho 287A) may each represent possible parent magma compositions. The VLT basalts could be formed by fractional crystallization of a picritic magma. The same magma could produce the population of Mg-rich pigeonite and anorthite grains occurring among mineral fragments. The low-Ti basaltic rocks could be related to the low-pressure fractionation of low-Ti melts. Compositional differences among the possible parent melts may be the result of mantle heterogeneities and/or assimilation processes. In the latter case, the low-Ti and Dho 287A melts might be hybrid compositions resulting from assimilation of KREEP by a picritic magma. Such a model would seem to be compatible with the geochemical and isotopic characteristics of Dho 287 basaltic rocks.

Thus, the Dho 287B breccia contains samples from

several magma eruptions, each different in composition, formation conditions, and cooling history. The abundant mare lithologies and the presence of the KREEP component suggest that Dho 287 was ejected from a region located distal to highland terrains, possibly from the western limb of the lunar nearside dominated by mare basalts and KREEP rocks.

Acknowledgments–Allan Patchen is thanked for his assistance with the electron microprobe analyses. Critical and constructive reviews by Marc Norman and an anonymous reviewer aided substantially to enhance the quality of this manuscript. The support of NASA grants from the Joint United States/ Russia Research in Space Sciences (JURRISS) and the Cosmochemistry Programs (NAG 5–1014 and NAG 5–11558) are gratefully acknowledged. S. I. Demidova and M. A. Nazarov were also supported by RFBR grant 02–05–64981.

Editorial Handling—Dr. Ross Taylor

REFERENCES

Anand M., Taylor L. A., Misra K. C., Demidova S. I., and Nazarov M. A. 2003a. KREEPy lunar meteorite Dhofar 287A: A new lunar mare basalt. *Meteoritics & Planetary Science.* This issue.

Anand M., Taylor L. A., Neal C. R., Snyder G. A., Patchen A., Sano Y., and Terada K. 2003b. Petrogenesis of lunar meteorite EET 96008. *Geochimica et Consmochimica Acta* 67(17).

Arai T. and Warren P. H. 1999. Lunar meteorite Queen Alexandra Range 94281: Glass composition and other evidence for launch pairing with Yamato-793274. *Meteoritics & Planetary Science* 34:209–235.

Arai T., Takeda H., and Warren P. H. 1996. Four lunar mare meteorites: Crystallization trends of pyroxenes and spinels. *Meteoritics & Planetary Science* 31:877–892.

Ariskin A. A., Petaev M. I., Borisov A. A., and Barmina G. S. 1997. METEOMOD: A numerical model for the calculation of melting-crystallization relationships in meteoritic igneous systems. *Meteoritics & Planetary Science* 32:123–133.

Cahill J. T., Floss C., Taylor L. A., Nazarov M. A., Anand M., and Cohen B. Forthcoming. Mineralogy, petrography, and geochemistry of hot desert lunar highland meteorites Dhofar 025, Dhofar 081, Dar al Gani 262, and Dar al Gani 400. *Meteoritics & Planetary Science.*

Delano J. W. 1986. Pristine lunar glasses: Criteria, data and implications. Proceedings, 16th Lunar and Planetary Science Conference. pp. 201–213.

Delano J. W. and Livi K. 1981. Lunar volcanic glasses and their constraints on mare petrogenesis. *Geochimica et Cosmochimica Acta* 45:2137–2149.

Demidova S. I., Nazarov M. A., Anand M., and Taylor L. A. 2002. Clast population of lunar regolith breccia Dhofar 287B (abstract #1290). 33rd Lunar and Planetary Science Conference. CD-ROM.

Goldstein J. I. and Axon H. J. 1972. Metallic particles from 3 Apollo 15 soils. In *The Apollo 15 lunar samples.* Houston: Lunar Science Institute. pp. 78–81.

Green D. H., Ringwood A. E., Ware N. G., Hibberson W. O., and Major A. 1971a. Experimental petrology and petrogenesis of Apollo 12 basalts. Proceedings, 2nd Lunar and Planetary Science Conference. pp. 601–615.

Green D. H., Ware N. G., Hibberson W. O., and Major A. 1971b. Experimental petrology of Apollo 12 mare basalts. Part I, sample 12009. *Earth and Planetary Science Letters* 13:85–96.

Grove T. L. and Bence A. E. 1977. Experimental study of pyroxene-liquid interaction in quartz-normative basalt 15597. Proceedings, 8th Lunar and Planetary Science Conference. pp. 1549–1579.

Grove T. L. and Lindsley D. H. 1978. Compositional variation and origin of lunar ultramafic green glasses. Proceedings, 9th Lunar and Planetary Science Conference. pp. 430–432.

Grove T. L. and Vaniman D. T. 1978. Experimental petrology of very low-Ti (VLT) basalts. In *Mare Crisium: The view from Luna 24*, edited by Merril R. B. and Papike J. J. New York: Pergamon Press. pp. 445–471.

Haggerty S. E. 1978. Luna 24: Systematics in spinel mineral chemistry in the context of an intrusive petrogenetic grid. In *Mare Crisium: The view from Luna 24*, edited by Merril R. B. and Papike J. J. New York: Pergamon Press. pp. 523–535.

Papike J., Taylor, L. and Simon S. 1991. Lunar minerals. In *Lunar sourcebook: A users guide to the Moon*, edited by Heiken G. H., Vaniman, D. T., and French B. M. Cambridge: Cambridge University Press. pp. 121–182.

Irving A. J. 1977. Chemical variation and fractionation of KREEP basalt magmas. Proceedings, 8th Lunar and Planetary Science Conference. pp. 2433–2448.

Joliff B. L. 1991. Fragments of quartz monzodiorite and felsite in Apollo 14 soil particles. Proceedings, 21st Lunar and Planetary Science Conference. pp. 101–118.

Ma M. S., Schmitt R. A., Taylor G. J., Warner R. D., Lange D. E., and Keil K. 1978. Chemistry and petrology of Luna 24 lithic fragments and <250 μm soils: Constraints on the origin of VLT mare basalts. In *Mare crisium: The view from Luna 24*, edited by Merril R. B. and Papike J. J. New York: Pergamon Press. pp. 569–592.

Marvin U. B., Lindstrom M. M., Holmberg B. B., and Martinez R. R. 1991. New observations on the quartz monzodiorite-granite suite. Proceedings, 21st Lunar and Planetary Science Conference. pp. 119–135.

Neal C. R. and Taylor L. A. 1992. Petrogenesis of mare basalts: A record of lunar volcanism. *Geochimica et Cosmochimica Acta* 56:2177–2211.

Papike J. J. and Vaniman D. T. 1978. Luna 24 ferrobasalts and the mare basalt suite: Comparative chemistry, mineralogy, and petrology. In *Mare Crisium: The view from Luna 24*, edited by Merril R. B. and Papike J. J. New York: Pergamon Press. pp. 371–401.

Papp H. A., Steele I. M., and Smith J. V. 1978. Luna 24: 90–150 micrometer fraction: Implication for remote sampling of regolith. In *Mare Crisium: The view from Luna 24*, edited by Merril R. B. and Papike J. J. New York: Pergamon Press. pp. 245–264.

Ringwood A. E. and Kesson S. E. 1976. A dynamic model for mare basalt petrogenesis. Proceedings, 7th Lunar and Planetary Science Conference. pp. 1697–1722.

Ryder G. and Marvin U. B. 1978. On the origin of Luna 24 basalts and soils. In *Mare Crisium: The view from Luna 24*, edited by Merril R. B. and Papike J. J. New York: Pergamon Press. pp. 339–356.

Shih C. Y., Nyquist L. E., Reese Y., Wiesmann H., Nazarov M. A., and Taylor L. A. 2002. The chronology and petrogenesis of the mare basalt clast from lunar meteorite Dhofar 287: Rb-Sr and Sm-Nd isotopic studies (abstract #1344). 33rd Lunar and Planetary Science Conference. CD-ROM.

Steele A. M., Colson R. O., Korotev R. L., and Haskin L. A. 1992. Apollo 15 green glass: Compositional distribution and petrogenesis. *Geochimica et Cosmochimica Acta* 56:4075–4090.

Stöffler D. and Knöll H. D. 1977. Composition and origin of plagioclase, pyroxene, and olivine clasts of lunar breccias 14006, 14063, 14066, 14311, 14320, and 14321. Proceedings, 8th Lunar

and Planetary Science Conference. pp. 1849–1867.
Tanton L. T. E., Van Orman J. A., Hager B. H., and Grove T. L. 2002. Re-examination of the lunar magma ocean cumulate overturn hypothesis: Melting or mixing is required. *Earth and Planetary Science Letters* 196:239–249.
Taylor L. A., Nazarov M. A., Demidova S. I., and Patchen A. 2001. A new lunar mare basalt from Oman. *Meteoritics & Planetary Science* 36:A204.
Walker D., Longhi J., and Hays J. F. 1972. Experimental petrology and origin of the Fra Mauro rocks and soil. Proceedings, 3rd Lunar and Planetary Science Conference. pp. 797–817.
Walker D., Longhi J., Lasaga A. C., Stolper E. M., Grove T. L., and Hays J. F. 1977. Slowly cooled microgabbros 15555 and 15065. Proceedings, 8th Lunar and Planetary Science Conference. pp. 1521–1547.
Warren P. H. and Wasson J. T. 1979. Effects of pressure on the crystallization of a "chondritic" magma ocean and implications for the bulk composition of the moon. Proceedings, 10th Lunar and Planetary Science Conference. pp. 2051–2083.
Wieczorek M. and Phillips R. 2000. The Procellarum KREEP terrane: Implications for mare volcanism and lunar evolution. *Journal of Geophysical Research* 105:20417–20430.